J Solid State Electrochem (2011) 15:2205–2211
DOI 10.1007/s10008-010-1237-z

ORIGINAL PAPER

Electrical properties of the protonic conductor 1 mol% Y-doped $BaZrO_{3-\delta}$

Hee Jung Park

Received: 28 September 2010 / Revised: 3 November 2010 / Accepted: 4 November 2010 / Published online: 17 November 2010

Abstract Much attention has been paid to barium zirconates because their high protonic conductivity and chemical stability are excellent properties for solid electrolytes. However, most studies have focused on highly doped materials such as 10 or 20 mol% Y-doped barium zirconates. In this study, the bulk and the grain boundary electrical properties of 1 mol% Y-doped barium zirconate are investigated as a function of temperature, water partial pressure, and oxygen partial pressure. At low temperatures and in wet atmospheres, the bulk of the barium zirconate predominantly conducts protonic defects, whereas, at high temperatures and in dry conditions, it is mixed oxygen ionic and electron-hole conducting. In the grain boundary, the protonic conductivity is a few orders of magnitude lower than the protonic conductivity in the bulk. In this study, possible causes for the low protonic conduction at the grain boundaries are considered.

Keywords Protonic conductor · Electrical property · Barium zirconate · Bulk · Grain boundary

Introduction

Solid oxide ionic conductors have recently attracted much interest as solid electrolytes (SEs) for solid oxide fuel cells (SOFC) due to their potential applications in green plants for producing electricity with hydrogen [1–3]. Among the ionic conductors, high temperature protonic conducting perovskites are viable SEs due to their high protonic conductivity at temperature of interest (400~700 °C). In particular, barium zirconates have been extensively studied because they possess both high protonic conductivity and thermodynamic stability [4–10]. For examples, K.D. Kreuer has studied the mobility and stability of the protonic charge carriers of the barium zirconates depending on water partial pressure (P_{H_2O}) [4]. K. Nomura and H. Kageyama have investigated their bulk transport in various thermodynamic conditions [5]. A.K. Azad et al. have even presented that the protonic conduction of the barium zirconates can change with their crystal structures [7]. As for the grain boundary (gb) conduction, C. KjØlseth et. al. have carefully considered if the space charge of the gb works for the gb conduction [8]. However, most studies have been focused on highly doped barium zirconates, i.e., $BaZr_{0.9}Y_{0.1}O_{3-\delta}$ or $BaZr_{0.8}Y_{0.2}O_{3-\delta}$, in which the electrical nature of the bulk and gb existing in polycrystalline barium zirconates is difficult to understand [3, 4, 11]. This is attributed to the following two facts. First, highly doped materials in the bulk show a strong association between positive charge carriers ($OH_O^{\bullet}$ and $V_O^{\bullet\bullet}$) and a dopant (Y'_{Zr}), and the materials often exhibit defect ordering [4, 12–14]. Second, they often lead the poor sinterability of the barium zirconates, and thus, closed pores existing in the grain boundaries hinder protonic transfer across the grain boundaries [11, 15, 16].

In this study, 1 mol% Y-doped $BaZrO_3$ ($BaZr_{0.99}Y_{0.01}O_{3-\delta}$, BZYO-1) with a high relative density (>95%) is intentionally selected as a representative low-doping material to understand the electrical nature of barium zirconates. In the following, its electrical properties as a function of temperature (T), water partial pressure (P_{H_2O}), and oxygen partial pressure (P_{O_2}) are presented.

H. J. Park (✉)
Samsung Advanced Institute of Technology (SAIT),
14-1 Nongseo-dong,
Yongin-si, Gyunggi-do 446-712, South Korea
e-mail: hj2007.park@samsung.com

Defect models

Electrical property of barium zirconates

Acceptor-doped barium zirconates can show oxygen ionic, electron-hole, and protonic conductivities as surroundings.

The red-ox reaction given below gives the electron-hole and the oxygen vacancies in an oxygen atmosphere. (Hereafter, the Kröger–Vink notation is used for point defects).

$$1/2O_2 + V_{O\leftarrow}^{\bullet\bullet} \rightarrow O_O^x + 2h^{\bullet} \quad (1)$$

Of course, an oxygen vacancy is also produced by acceptor doping.

$$YO_{1.5} \xrightarrow{ZrO_2} Y'_{Zr} + 1/2V_O^{\bullet\bullet} + 3/2O_O^x \quad (2)$$

In wet environments, on the other hand, protonic defects are predominantly generated from Eq. 3.

$$H_2O + 2h^{\bullet} + 2O_{O\leftarrow}^x \rightarrow 2OH^{\bullet} + 1/2O_2 \quad (3)$$

The following protonic defect reaction is obtained from Eqs. 1 and 3.

$$H_2O + V_O^{\bullet\bullet} + O_{O\leftarrow}^x \rightarrow 2OH^{\bullet} \quad (4a)$$

$$K = [OH_O^{\bullet}]^2 / P_{H_2O}[V_O^{\bullet\bullet}][O_O] \quad (4b)$$

where K denotes the equilibrium constant of Eq. 4a.

Accordingly, the total conductivity (σ_{total}) of the barium zirconates is affected by the protonic, the oxygen ionic, and the electron-hole conductivities. (Note that the dopant is immobile at the temperature of interest). The total conductivity is given by

$$\sigma_{total} = \sigma_{OH^{\bullet}} + \sigma_{V^{\bullet\bullet}} + \sigma_{h^{\bullet}} \quad (5)$$

where $\sigma_{OH^{\bullet}}$, $\sigma_{V^{\bullet\bullet}}$, and $\sigma_{h^{\bullet}}$ are the protonic, the oxygen ionic, and the electron-hole conductivities, respectively.

The protonic conduction depending on P_{H_2O}

The protonic conduction may depend on P_{H_2O} because it is enabled by the introduction of water. The dependency, however, varies with electroneutrality condition (ENC). The ENC in barium zirconates can be written as

$$\left[OH_O^{\bullet}\right] + 2\left[V_O^{\bullet\bullet}\right] + \left[h^{\bullet}\right] = \left[Y'_{Zr}\right]. \quad (6)$$

In a certain thermodynamic region, if the ENC is equal to $2\left[V_O^{\bullet\bullet}\right] \sim \left[Y'_{Zr}\right]$, the protonic conduction depends on $P_{H_2O}^{1/2}$; whereas, if the ENC is $\left[OH_O^{\bullet}\right] \sim \left[Y'_{Zr}\right]$, it does not depend on P_{H_2O} (refer to the "Appendix"). In the case that the ENC is $2\left[V_O^{\bullet\bullet}\right] + \left[OH_O^{\bullet}\right] \approx \left[Y'_{Zr}\right]$, the protonic defect and corresponding conduction depend on $P_{H_2O}^{0\sim1/2}$ (see the "Appendix").

Experimental procedure

BZYO-1 was synthesized using the Pechini method with appropriate amounts of $Ba(NO_3)_2$ (99.99%, Sigma Aldrich), $ZrO(NO_3)_2 \cdot 6H_2O$ (>99.99%, Sigma Aldrich), and $Y(NO_3)_3 \cdot 6H_2O$ (99.9%, Sigma Aldrich) as reactants. The reactants were dissolved in an aqueous solution, and then ethylene glycol was added to the solution. The solution was heated to 200 °C and stirred to produce the precursor powders. The obtained precursor powders were calcinated at 1,100 °C for 3 h and then ground and pressed into a pellet. Finally, the pellets were placed in a cold-isostatic press at 300 MPa. The synthesized BZYO-1 powders were characterized by X-ray diffraction (XRD). The pellet was sintered at 1,700 °C for 24 h in air. The relative density of the sintered pellet was estimated using the Archimedean method to be >95%. The chemical compositions and the concentrations of background impurities, including Ca and Si, which are able to form glassy phases in the gb, were determined by inductively coupled plasma emission spectroscopy (ICP, see Table 1). The microstructure and the grain size of the pellet were examined using a scanning electron microscope (SEM) and a high-resolution transmission electron microscope (HR-TEM, JEOL).

For the electrical measurements, the surface of the sintered pellet, with a diameter of 0.6 cm and thickness 0.12 cm, was polished by using SiC-paper, and then Pt-paste was painted onto both surfaces. After that, the pellet was thermally treated at 800 °C for 1 h in air. The electrical resistance of the pellet was measured as a function of temperature (T=270–850 °C) by using 2-probe ac impedance spectroscopy in dry ($P_{H_2O} < 1 \times 10^{-4}$atm and $Po_2 \sim 3 \times 10^{-6}$atm) and wet N_2 ($P_{H_2O} \sim 2.3 \times 10^{-2}$atm and $Po_2 \sim 3 \times 10^{-6}$atm). Dry N_2 gas also contains water due to impurities (P_{H_2O}<100 ppm) in the gas cylinder. Thus, "dry" means nominally dry. The electrical resistance was also examined as a function of

Table 1 The concentrations of Si and Ca and Ba, Zr, and Y (dopant) in a sintered $BaZr_{0.99}Y_{0.01}O_{3-\delta}$ (BZYO-1) determined using the ICP technique

Component	Concentration (ppm)
Ba	997,490
Zr	991,830
Y	10,700
Si	150
Ca	240

$P_{H_2O}(0.01\ \text{atm} < P_{H_2O} < 0.03\ \text{atm})$ or $Po_2\left(1 \sim 3 \times 10^{-6}\text{atm}\right)$. P_{H_2O} was obtained by passing N_2 through an isothermal bath containing water at controlled temperature (8~24 °C). Po_2 was controlled by mixing of O_2 and N_2, and it was checked with a zirconia oxygen sensor. The impedance spectra were obtained in the frequency range from 0.05 Hz to 10 MHz using an impedance analyzer (Novocontrol). Amplitude for the measurements was 50 mV. For the fitting of the data, Z-view program (Scribner Associates) was used.

Results and discussion

XRD, SEM, and ac impedance

Figure 1 shows the XRD patterns of BZYO-1 powders obtained after calcination and sintering. Each individual peak was indexed with the JCPDS card of barium zirconate with a perovskite structure. A single phase after calcination and sintering was well formed. The lattice parameter calculated from the peak positions calibrated with an internal quartz reference was ~0.4187±0.0002 nm.

The microstructure and the grain size of BZYO-1 were examined using a scanning electron microscope (Fig. 2). It was dense, as expected. Its average grain size was estimated to be ~3.5 μm, showing that it is much higher than those of the reported high-doping barium zirconates (note that they present a grain size of few hundred of nanometers) [6, 10]. The grain size was determined measuring the number of grain boundary intercepts per unit test line.

Figure 3 shows the typical impedance spectra of BZYO-1 at 450 °C in dry and wet N_2. The inset shows the spectra in higher frequency region (near the starting point of Fig. 3), showing that another semicircle exists (note that

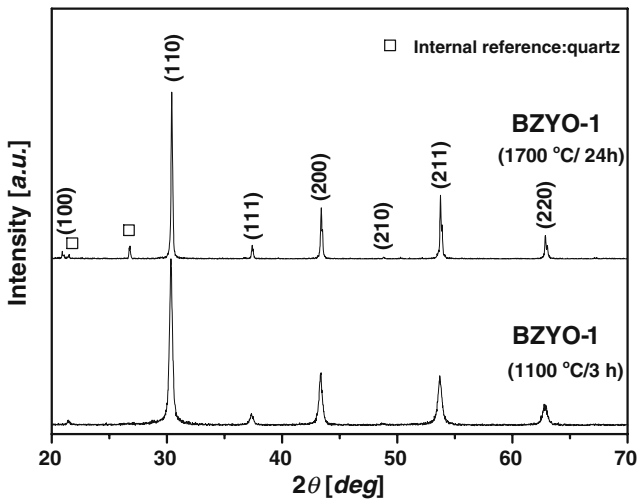

Fig. 1 XRD patterns of $BaZr_{0.99}Y_{0.01}O_{3-\delta}(\text{BZYO}-1)$ after calcination (1,100 °C for 3 h) and sintering (1,700 °C for 24 h)

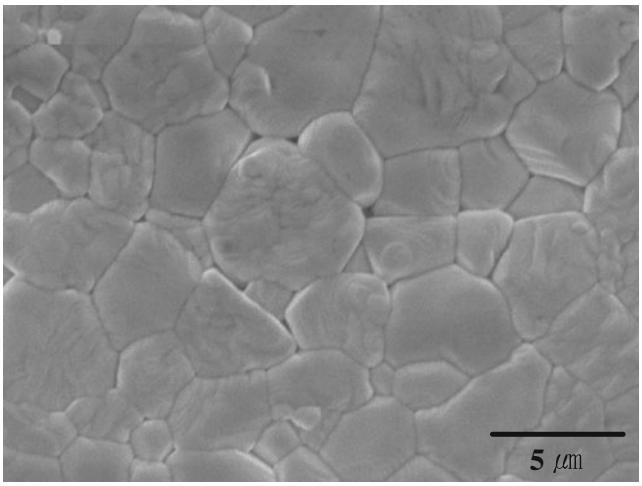

Fig. 2 An image of the polished surface of $BaZr_{0.99}Y_{0.01}O_{3-\delta}(\text{BZYO}-1)$ pellet obtained using scanning electron microscopy (SEM)

two semicircles are visible up to high temperature ~694 °C). Two parallel RQ circuits in series were employed to fit the data (i.e., $R_{bulk}Q_{bulk}$ and $R_{gb}Q_{gb}$ with the subscripts bulk and gb denoting the bulk and gb, respectively. R is the resistance and Q is a constant phase element given as $C = (R^{1-n}Q)^{1/n}$). The values of C_{bulk} and C_{gb} obtained from the sample are $\sim 1\times10^{-11}$ and $\sim 1\times10^{-9}$ F, respectively. The dielectric constant (ε) estimated from the C_{bulk} is ~46 agreed reasonably well with the value (ε~15) measured for nominally pure barium zirconate, indicating that the semicircular arc appeared in the higher

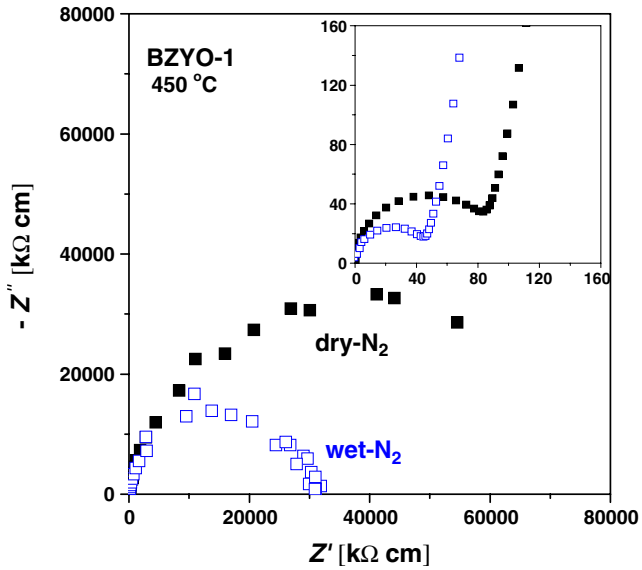

Fig. 3 Impedance patterns of $BaZr_{0.99}Y_{0.01}O_{3-\delta}$ (BZYO-1) in dry and wet N_2 at 450 °C. The *inset* shows the spectra in the high frequency region. The *first* (high frequency part) and *second* (low frequency part) *semicircles* correspond to the bulk and grain boundary, respectively

frequency region represents the bulk [17]. As seen, the resistances of the bulk and the gb decreased in wet conditions, which shows that the protonic conduction is enabled by water incorporation.

Bulk conduction

The bulk conductivities (σ_{bulk}) estimated from the impedance patterns are shown as a function of temperature in dry and wet N_2 (circle and square symbol, respectively) in Fig. 4.

In wet N_2, the bulk conductivity is much higher than that in dry N_2 below 500 °C, whereas the behavior above 500 °C is reversed. This is because the dominant charge carrier and the corresponding conductivity change with the temperature and water partial pressure. Kuz'min et. al. have reported that the electron-hole mainly conducts in high Po_2 and dry condition while both the electron-hole and the ionic charge carriers dominantly conduct in low Po_2 and humid condition [9].

Below 500 °C and in wet N_2, the dominant conduction is protonic, that is, $\sigma_{total} \sim \sigma_{OH^\bullet}$ in Eq. 6 (here, σ_{total} is equal to σ_{bulk} in Fig. 4) because the activation energy (E_a~0.4 eV) is very close to the traditional value of the protonic conduction [4] and the measured data are well matched with the estimated protonic conductivity (the solid curved line in Fig. 4). The estimated conductivity was obtained using the following Nernst–Einstein equation.

$$\sigma_{OH^\bullet} = \left[OH_O^\bullet\right] e^2 D_{OH_O^\bullet} / k_B T \quad (7)$$

where $D_{OH^\bullet}$ indicates the diffusivity of the protonic defect, and e and k_B denote the elementary electronic charge and the Boltzmann constant, respectively. To calculate $\sigma_{OH^\bullet}$, Eq. A4, which gives the protonic defect concentration ($\left[OH_O^\bullet\right]$), and the diffusivity reported by Kreuer were used (the diffusivity and the value of K (the equilibrium constant) in Eq. A4 are assumed to be the same with the reported one of 2 mol% Y-doped $BaZrO_3$) [18]. Such a great match between the measured data and the estimated value (270~500 °C) indicates that the sample was fully equilibrated with the gaseous water, and the ENC of the bulk in this region is $2\left[V_O^{\bullet\bullet}\right] + \left[OH_O^\bullet\right] \approx \left[Y_{Zr}'\right]$ using Eq. A4a as the protonic defect concentration in Eq. 7. This is also supported by the P_{H_2O} dependence of $\sigma_{OH^\bullet}$. (See Fig. 5. $\sigma_{OH^\bullet}$ is dependent on $P_{H_2O}^{0\sim1/2}$ rather than $P_{H_2O}^{0}$ or $P_{H_2O}^{1/2}$, meaning that $\sigma_{OH^\bullet}$ is governed by the ENC, $2\left[V_O^{\bullet\bullet}\right] + \left[OH_O^\bullet\right] \approx \left[Y_{Zr}'\right]$).

One the other hand, in dry N_2 of Fig. 4, $\sigma_{OH^\bullet}$ drastically decreases due to the dehydration of water (note $\left[OH_O^\bullet\right]$ decreases with the decrease of P_{H_2O}). Accordingly, $\sigma_{V^{\bullet\bullet}} + \sigma_{h^\bullet}$ increases. (Note that the concentration of the oxygen vacancy and the electron-hole increases as the protonic defect decreases according to Eq. 6). This behavior becomes clear above 500 °C. The measured conductivity in the dry condition increases with temperature and finally becomes higher than that in the wet condition. This indicates that the dominant conduction is no longer protonic conduction at high temperatures. The activation energy (E_a) of σ_{bulk} in dry condition is also high to be ~0.95 eV compared with that of σ_{bulk} in wet condition (see Fig. 4). This value is in the middle of the reported activation energies of the electron-hole and the oxygen vacancy conduction, implying that BZYO-1 becomes mixed oxygen ionic and electron-hole conducting at high temperatures and in dry condition (it has been reported that the activation

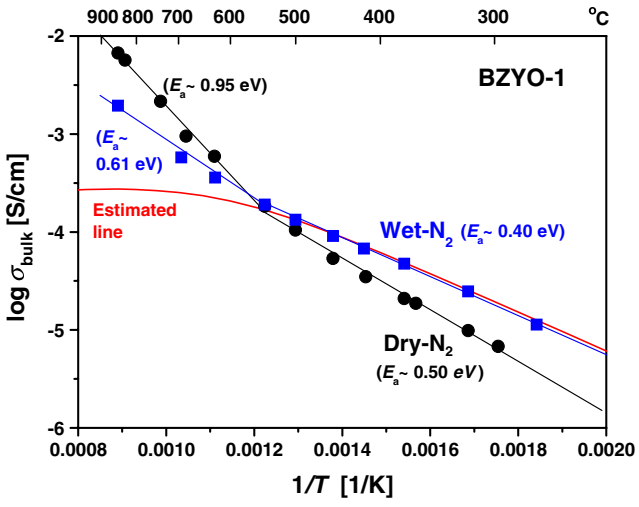

Fig. 4 The temperature dependence of the bulk conductivity (σ_{bulk}) in dry and wet N_2. The *curved solid line* is the estimated protonic conductivity

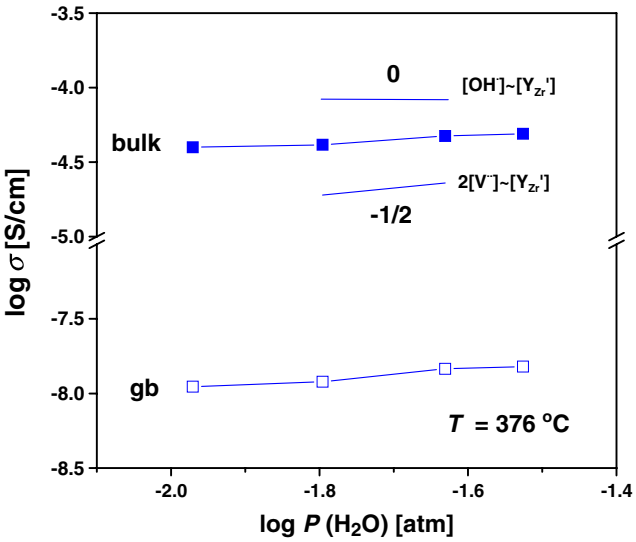

Fig. 5 The water partial pressure (P_{H_2O})-dependence of the bulk and gb conductivities at 376 °C

energies of $\sigma_{h\bullet}$ and $\sigma_{V\bullet\bullet}$ are ~0.87 eV and ~1.1 eV, respectively) [9, 19]. Such results are supported by previously reported results. Nomura and Kageyama have shown in dry atmosphere that both the oxygen vacancy and the electron-hole are dominant charge carriers [5]. Kuz'min et al. have also presented that the mixed ionic and electron-hole conduction governs the total conduction in the middle of $Po_2\left(10^{-4}\text{ atm} < Po_2 < 10^{-10}\text{ atm}\right)$, while the electron-hole conduction is predominant in high Po_2 (in air) and dry atmosphere [9]. This mixed conduction in dry condition is confirmed again by the Po_2 dependence of σ_{bulk} as follows.

The Po_2 dependence of σ_{bulk} at 740 °C is exhibited in Fig. 6. As seen in the figure, the measured conductivity weakly depends on Po_2, meaning that σ_{bulk} consists of $\sigma_{V\bullet\bullet}$ and $\sigma_{h\bullet}$. To separately obtain $\sigma_{V\bullet\bullet}$ and$\sigma_{h\bullet}$, the measured conductivity was numerically fitted using the following typical equation.

$$\sigma_{total} = \sigma_{V\bullet\bullet} + \sigma^{o}_{h\bullet} Po_2{}^{1/4} \tag{8}$$

where $\sigma^{o}_{h\bullet}$ is $\sigma_{h\bullet}$ at Po_2=1 atm. (Note that $\sigma_{V\bullet\bullet}$ in this equation is independent on Po_2, as revealed in Eq. 2 . On the other hand, $\sigma_{h\bullet}$ does strongly depend on Po_2 as seen from Eq. 1 [20]). In Fig. 6, the curved solid line indicates the numerical best fit of the measured conductivity and the dotted lines denote the oxygen ionic and the electron-hole conductivities obtained from the fitting. The values of $\sigma_{V\bullet\bullet}$ and $\sigma^{o}_{h\bullet}$ obtained are ~0.0023 and ~0.0077 S/cm at 740 °C, respectively, implying that the bulk of the BZYO-1 at high temperatures and, in dry conditions, is surely mixed conducting. (The electron-hole transference number $t_{h\bullet} = \sigma_{h\bullet}/(\sigma_{V\bullet\bullet} + \sigma_{h\bullet})$ of BZYO-1 is inserted in Fig. 6).

Grain boundary conduction

The electrical properties of the gb in polycrystalline barium zirconates has attracted much attention because their protonic conductivity is markedly lower than that of the single crystal over a wide temperature range [4, 6]. In addition, nanostructured materials with large volume ratios of the gb have come into focus [21]. Thus, a better understanding of the origin of the electrical properties of the gb in the protonic conductors at a fundamental level has become important.

Figure 7 shows the gb conductivity (σ_{gb}) of BZYO-1 in dry and wet N_2 (circle and square symbols, respectively). The inset indicates the specific gb conductivity (i.e., the conductivity across a single gb, $\sigma^{sp}_{gb} = \sigma_{bulk}\left(\tau_{bulk}/\tau_{gb}\right)$ with τ=RC). In wet N_2, σ_{gb} is higher than that in dry N_2, indicating that the protonic conduction produced in the gb similar to that produced in the bulk and is the dominant conduction at lower temperatures (similarly, σ^{sp}_{gb} in wet N_2 is higher than that in dry N_2). However, $\sigma_{OH\bullet}$ in the gb is markedly lower than that in the bulk (for example, $\sigma^{sp}_{gb} \sim 10^{-9}$ S/cm, $\sigma_{bulk} \sim 7 \times 10^{-5}$ S/cm at 415 °C, respectively). The activation energy of $\sigma_{OH\bullet}$ (E_{gb}) is also high to be ~1.22 eV compared with that in the bulk (E_{bulk} ~0.40 eV). Such blocking has been similarly observed at highly doped barium zirconates [4, 6, 22]. Fabbri et al. have reported that σ_{gb} in 20~40 mol% Y-doped $BaZrO_3$ is lower than σ_{bulk}, and Duval et al. presented 3~4 orders of magnitude difference between the bulk conductivity and the specific gb conductivity.

This high resistance to protonic transport across the gb can be attributed to either extrinsic (impurities, pores) or intrinsic (space charge or structural effect) causes or both

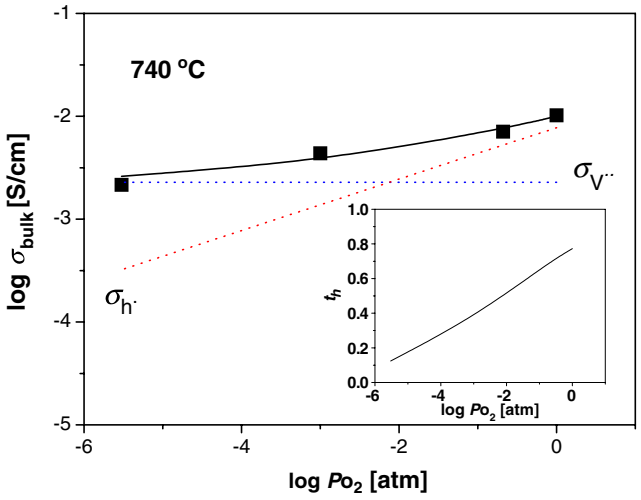

Fig. 6 The oxygen partial pressure (P_{O_2}) dependence of the bulk conductivity (σ_{bulk}) at 740 °C. The *inset* presents the electron-hole transference number (t_h) calculated from the electron-hole and the oxygen ionic conductivity ($\sigma_{h\bullet}$ and $\sigma_{V\bullet\bullet}$)

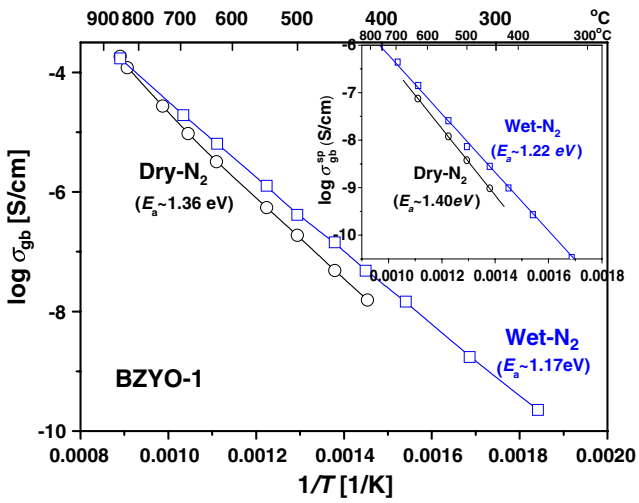

Fig. 7 The temperature dependence of the gb conductivity (σ_{gb}) in dry and wet N_2. The *inset* shows the specific gb conductivity (i.e., the conductivity of a single gb, σ^{sp}_{gb})

[4, 22, 23]. As observed for conventional SEs, impurities such as silicates segregate into grain boundary cores (which are structurally different regions from the bulk) to form layers of an insulating amorphous phase which at least partially block the current (i.e., cause current constriction) [24]. This constriction resistance, however, may not fully explain the blocking effects of the gb because the sample is nearly free of the amorphous phase (see the result of the ICP measurement in Table 1 and a HR-TEM image (Fig. 8)) and the fact that σ_{gb} depends on P_{H_2O} (see Fig. 5). More emphasis, therefore, should be placed on possible intrinsic causes rather than (or in addition to) such extrinsic mechanisms.

A crystal structure has been regarded as the most important parameter in protonic motion, which includes both mobility and concentration of ionic charge carriers [25, 26]. Accordingly, the structural effects in the gb are readily considered since the gb has often structural lattice distortion and a large number of strained or missing bonds leading to the change of the concentration and mobility of charge carriers. Indeed, for the barium zirconate protonic conductor, Azad et al. have shown how sensitive its crystal structure is to the protonic conduction (the α-form of the barium zirconate exhibits a slightly smaller unit cell and much lower protonic conductivity than the β-form) [7]. In this study, the gb of BZYO-1 may also be structurally distorted as seen in Fig. 8 and, somehow, it may lead the high resistance of the gb. Of course, the space charge of the gb, a kind intrinsic cause, can be a main reason of the gb blocking. However, in BZYO-1, any evidences related to the space charge effect are not found. For example, the measured E_{gb} of Fig. 7 (~1.22 eV) does not match the E_{gb} (~0.75 eV) estimated with the gb space charge potential (~0.35 V), assuming Mott–Schottky situation (see the reference [27] where the equations for the calculation are described). Nevertheless, uncertainty about the origin of the gb resistance still remains due to a lack of study (note that the origin of the gb blocking is a hot topic and is still in debate). Recently, KjØlseth et al. have empirically shown that the space charge effect works on the gb conduction of the Y-doped barium zirconate [8]. Thus, more careful studies and analysis are required in order to clarify it.

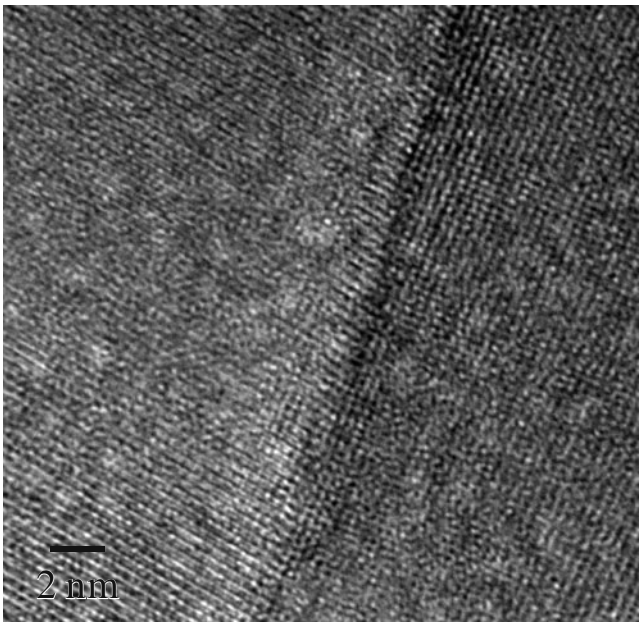

Fig. 8 A high-resolution transmission electron microscopy (HR-TEM) image of the bulk and grain boundary of BZYO-1

Conclusion

The electrical properties of 1 mol% Y-doped barium zirconate ($BaZr_{0.99}Y_{0.01}O_{3-\delta}$) were investigated as a function of temperature, water partial pressure, and oxygen partial pressure. The protonic conduction in the bulk is dominant at low temperatures and in wet atmospheres, but is significantly reduced at high temperatures and in dry conditions, leading to the increase of the oxygen vacancy and the electron-hole conduction. The protonic conductivity of the grain boundary was much lower than that of the bulk. Possible causes for the low protonic transport in the grain boundaries were considered.

Acknowledgment I thank Prof. Sangtae Kim for the valuable discussions and study and Dr. Chan Kwak for the SOFC project.

Appendix

The P_{H_2O}-dependence of the protonic conductivity is defined as the *ENC*. I consider three cases.

(1) *ENC*: $2\left[V_O^{\bullet\bullet}\right] \approx \left[Y'_{Zr}\right]$

In this case, the protonic defect and the corresponding protonic conductivity strongly depend on the water partial pressure as shown below.

$$\left[OH_O^{\bullet}\right] = \left(K\left[V_O^{\bullet\bullet}\right][O_O]\right)^{1/2} P_{H_2O}^{1/2} \tag{A1}$$

$$\sigma_{OH^{\bullet}} = \left[OH_O^{\bullet}\right] e\mu_{OH^{\bullet}} \propto P_{H_2O}^{1/2} (c_{v\bullet\bullet} \sim \text{constant}). \tag{A2}$$

(2) *ENC*: $2\left[V_O^{\bullet\bullet}\right] + \left[OH_O^{\bullet}\right] \approx \left[Y'_{Zr}\right]$

In perovskite materials (ABO_3), the site restriction is given by

$$\left[V_O^{\bullet\bullet}\right] + \left[OH_O^{\bullet}\right] + \left[O_O^{x}\right] = 3. \quad \text{(A3)}$$

Considering Eq. A3 and Eq. 4, the protonic defect can be estimated as following.

$$\left[OH_O^{\bullet}\right] = \frac{3KP_{H_2O} - \sqrt{KP_{H_2O}(9KP_{H_2O} - 6KP_{H_2O}S + KP_{H_2O}S^2 + 24S - 4S^2}}{KP_{H_2O} - 4} \quad \text{(A4)}$$

where S denotes an effective dopant concentration (Ref. 4). Thus, in this condition,

$$\sigma_{OH^{\bullet}} = \left[OH_O^{\bullet}\right] e\mu_{OH^{\bullet}} \propto P_{H_2O}^{0\sim 1/2} \quad \text{(A5)}$$

(3) *ENC*: $\left[OH_O^{\bullet}\right] \approx \left[Y_{Zr}^{'}\right]$

The protonic conductivity hardly depends on the water partial pressure owing to the fixed concentration of the acceptor.

$$\left[OH_O^{\bullet}\right] = \left[Y_{Zr}^{'}\right] = \text{constant} \quad \text{(A6)}$$

$$\sigma_{OH^{\bullet}} = \left[OH_O^{\bullet}\right] e\mu_{OH^{\bullet}} \propto P_{H_2O}^{0} \quad \text{(A7)}$$

References

1. Norby T (1999) Solid State Ionics 125:1
2. Park HJ, Choa YH (2010) Electrochem Solid-State Lett 13:K49
3. Kreuer KD (1996) Chem Mater 8:610
4. Kreuer KD (2003) Annu Rev Mater Res 33:333
5. Nomura K, Kageyama H (2007) Solid State Ionics 178:661
6. Fabbri E, Pergolesi D, Licoccia S, Traversa E (2010) Solid State Ionics 181:1043
7. Azad AK, Savaniu C, Tao S, Duval S, Holtappels P, Ibberson RM, Irvine JTS (2008) J Mater Chem 18:3414
8. KjØlseth C, Fjeld H, Prytz Ø, Dahl PI, Estournes C, Haugsrud R, Norby T (2010) Solid State Ionics 181:268
9. Kuz'min AV, Balakireva VB, Plaksin SV, Gorelov VP (2009) Russ J Electrochem 12:1460
10. Yamazaki Y, Hernandez-Sanchez R, Haile SM (2009) Chem Mater 21:2755
11. Duval SBC, Holtappels P, Vogt UF, Stimming U, Graule T (2009) Fuel Cells 5:613
12. Wang JX, Su WH, Xu DP, He TM (2006) J Alloys Compd 421:45
13. Davis RA, Islam MS, Gale JD (1999) Solid State Ionics 126:323
14. Giannici F, Longo A, Kreuer KD, Balerna A, Martorana A (2010) Solid State Ionics 181:122
15. Bablio P, Haile SM (2005) J Am Ceram Soc 88(9):2362
16. Gao D, Guo R (2010) J Alloys Compd 493:288
17. Azad AM, Subramaniam S (2002) Mater Res Bull 37:11
18. Kreuer KD, Adams S, Münch W, Fuchs A, Klock U, Maier J (2001) Solid State Ionics 145:295
19. Bohn HG, Schober T (2000) J Am Ceram Soc 83:768
20. Park JY, Choi GM (2002) Solid State Ionics 154:535
21. Chen X, Rieth L, Miller MS, Solzbacher F (2009) Sens actuators B, Chem 137:578
22. Iguchi F, Sata N, Tsurui T, Yugami H (2007) Solid State Ionics 178:691
23. Bohn HG, Schober T, Mono T, Schilling W (1999) Solid State Ionics 117:219
24. Aoki M, Chiang YM, Kosacki I, Lee IJR, Tuller H, Liu YP (1996) J Am Ceram Soc 79:1169
25. Kreuer KD (1999) Solid State Ionics 125:285
26. Shi C, Yoshino M, Morinaga M (2005) Solid State Ionics 176:1091
27. Park HJ, Kim S (2007) J Phys Chem C 111:14903